

1 Supplementary Information

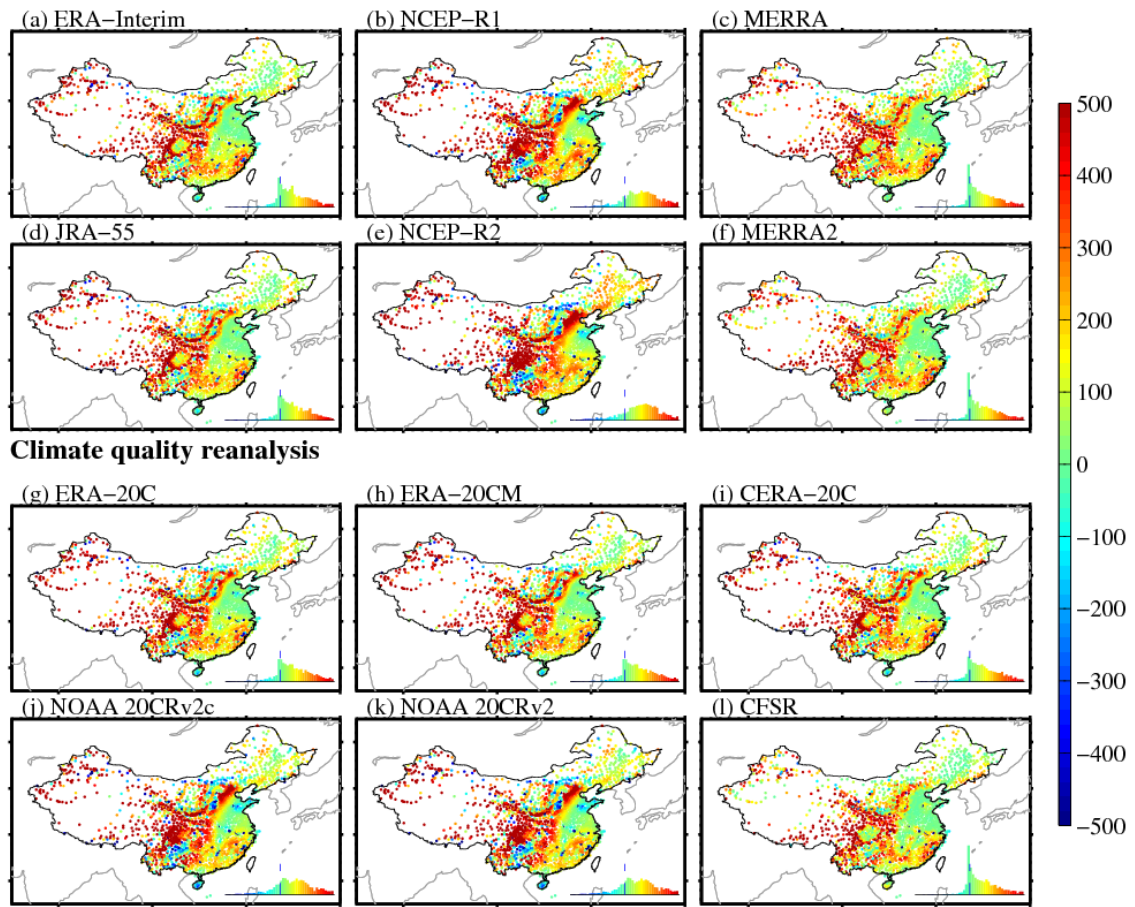
2 **On the Suitability of Current Atmospheric**  
3 **Reanalyses for Regional Warming Studies over China**

4  
5  
6  
7 Chunliè Zhou<sup>1</sup>, Yanyi He<sup>1</sup>, Kaicun Wang<sup>1\*</sup>

8 <sup>1</sup>College of Global Change and Earth System Science, Beijing Normal University,  
9 Beijing, 100875, China

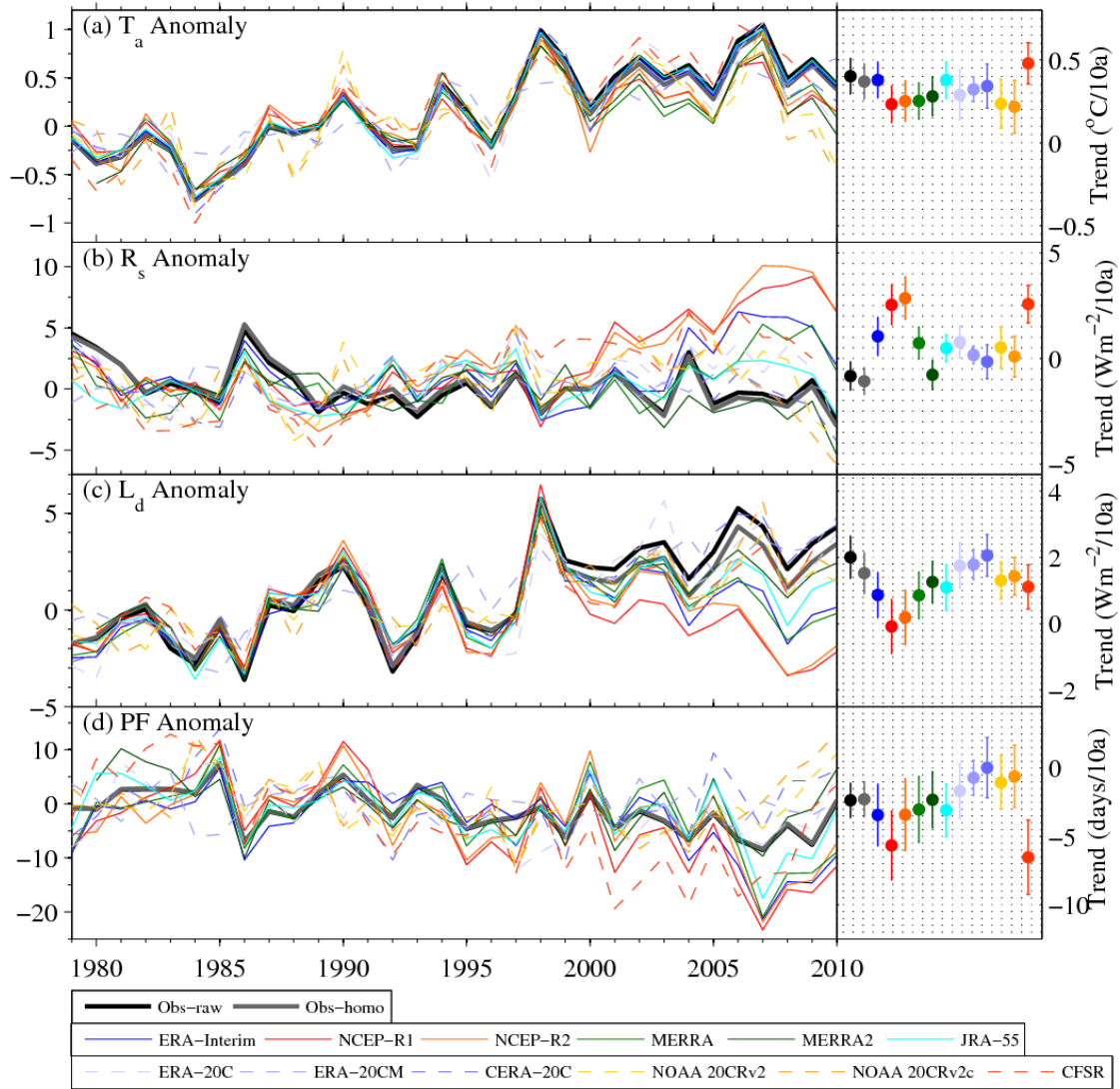
10  
11  
12  
13  
14  
15  
16  
17  
18  
19 The supplementary information includes twenty-three Figures S1-S23.

**Conventional NWP reanalysis**



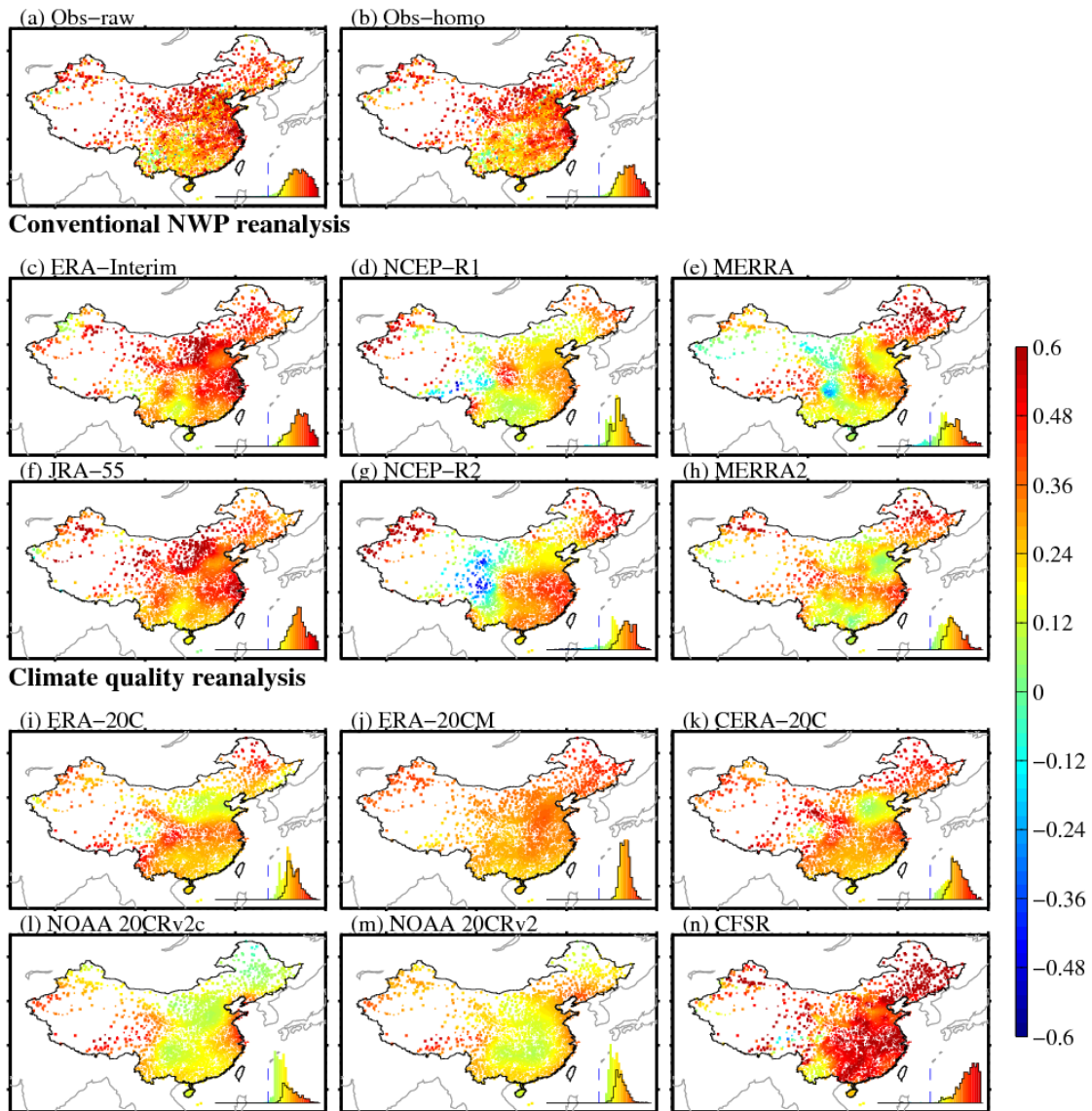
20

21 **Figure S1.** The elevation difference ( $\Delta$ Height, unit: m) between the model and  
22 observation stations. The information on model resolution is included in Table 1.

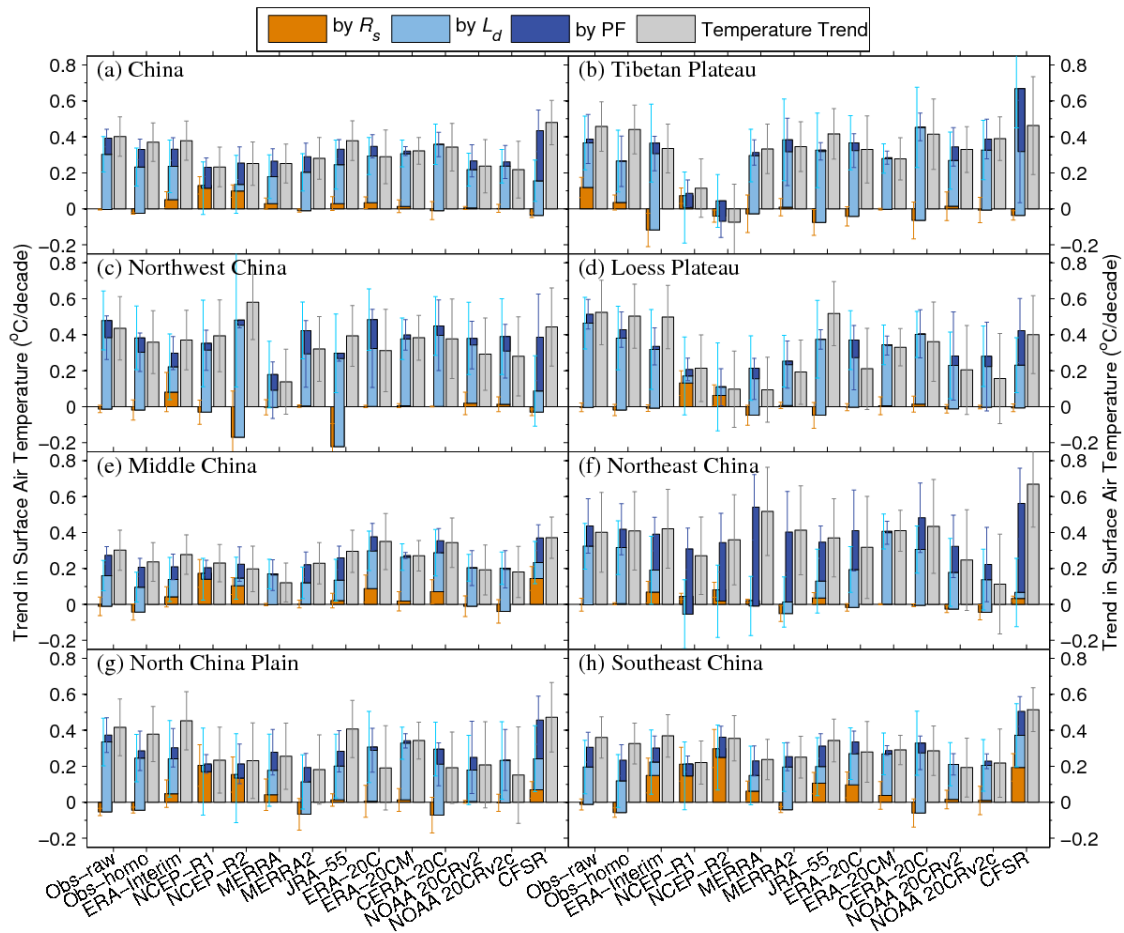


23

24 **Figure S2.** The time series of (a) surface air temperature anomaly ( $T_a$ ), (b) surface  
 25 incident solar radiation ( $R_s$ ), (c) surface downward longwave radiation ( $L_d$ ) and (d)  
 26 precipitation frequency anomaly (PF) with their trends (in right each) from the raw  
 27 observation, homogeneous observation and the twelve reanalysis products during the  
 28 period 1979-2010 over China. The error-bars show the 95% confident intervals of the  
 29 trends.

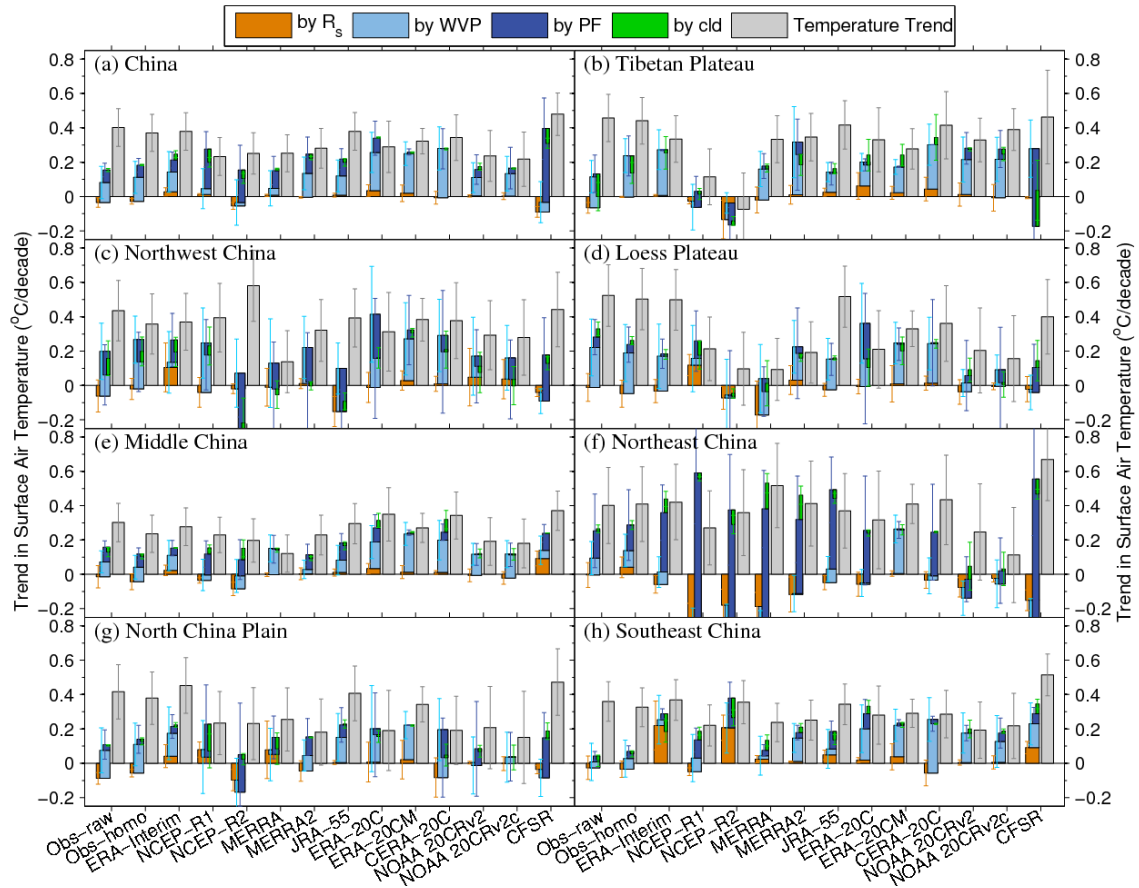


30  
 31 **Figure S3.** The trends in surface air temperature ( $T_a$ , unit:  $^{\circ}\text{C}/\text{decade}$ ) during the  
 32 period 1979–2010 from (a) raw observations, (b) homogeneous observations and the  
 33 twelve reanalysis products over China, i.e., (c) ERA-Interim, (d) NCEP-R1, (e)  
 34 MERRA, (f) JRA-55, (g) NCEP-R2, (h) MERRA2, (i) ERA-20C, (j) ERA-20CM, (k)  
 35 CERA-20C, (l) NOAA 20CRv2c, (m) NOAA 20CRv2 and (n) CFSR. The probability  
 36 distribution functions of all the trends are shown as colored histogram, and the black  
 37 stairs are integrated from the trends with a significance level of 0.05 (based on  
 38 two-tailed Student's  $t$ -test).



39

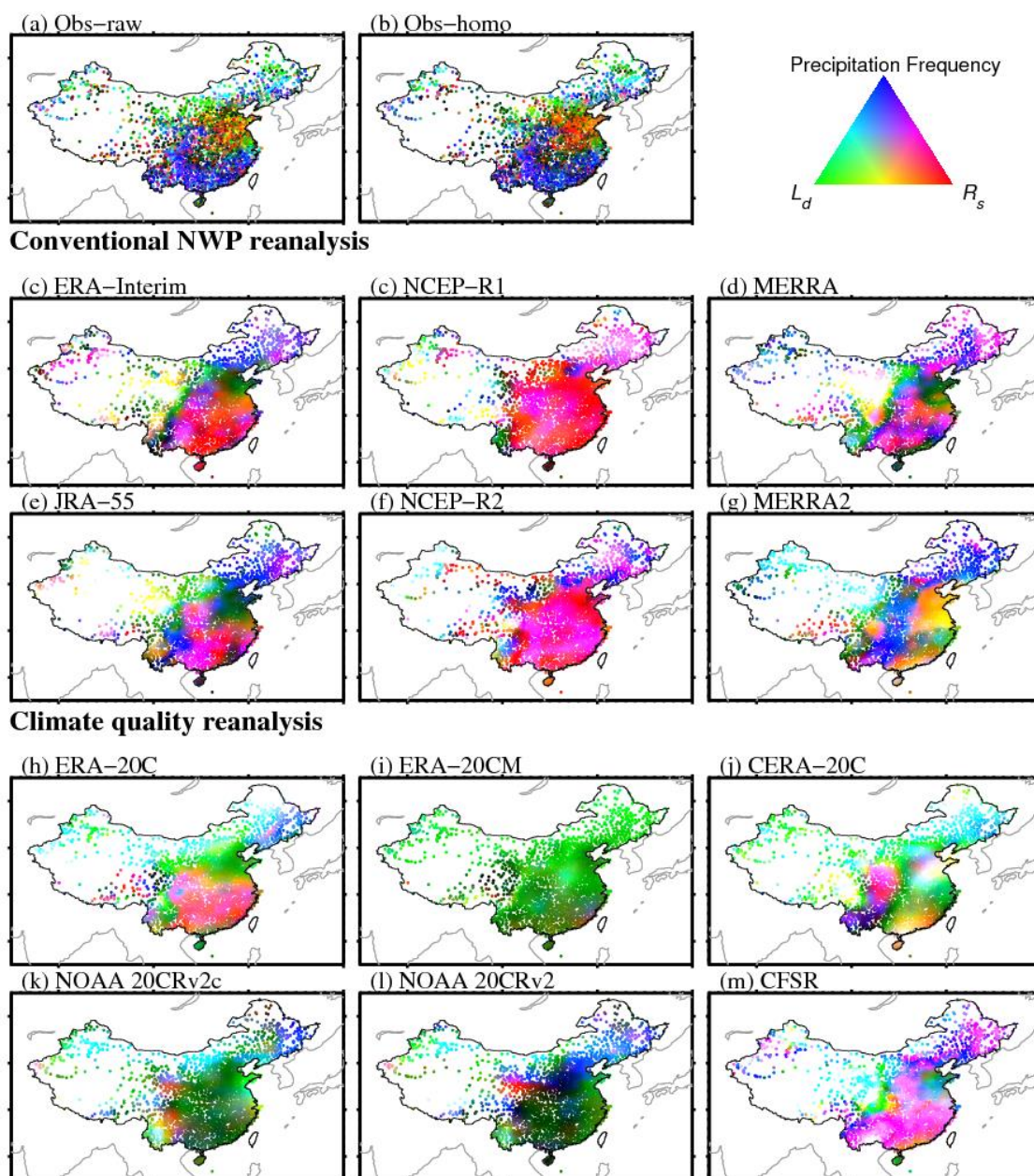
40 **Figure S4.** Contribution of trends in surface air temperature ( $T_a$ , unit:  $^{\circ}\text{C}/\text{decade}$ )  
 41 from three relevant parameters, i.e., surface incident solar radiation ( $R_s$ , in brown, unit:  
 42  $\text{W m}^{-2}/\text{decade}$ ), surface downward longwave radiation ( $L_d$ , in light blue, unit:  
 43  $\text{W m}^{-2}/\text{decade}$ ) and the precipitation frequency (PF, in deep blue, unit: days/decade)  
 44 during the period 1979-2010 in the raw observations, homogeneous observations and  
 45 the twelve reanalysis products over China and its seven subregions.



46

47 **Figure S5.** The same as Figure S4, but using the atmospheric water vapor and cloud

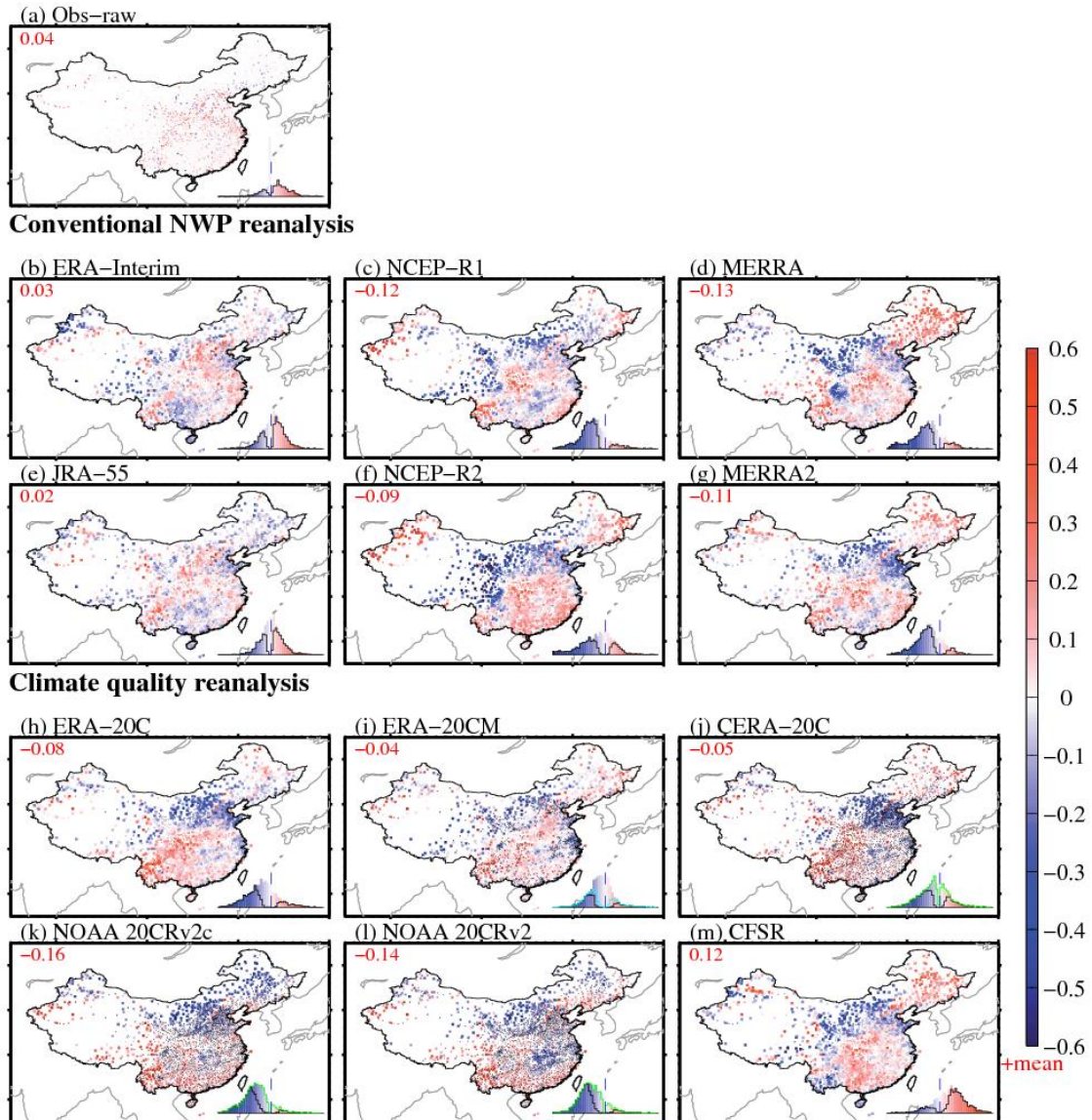
48 fraction instead of surface downward longwave radiation.



49

50 **Figure S6.** Composite map of contribution of trends in three relevant parameters  
 51 [surface incident solar radiation ( $R_s$ , in red), surface downward longwave radiation ( $L_d$ ,  
 52 in green) and the precipitation frequency (in blue)] to trends in surface air temperature  
 53 ( $T_a$ , unit:  $^{\circ}\text{C}/\text{decade}$ ) during the period 1979–2010 from (a) the raw observations, (b)  
 54 homogeneous observations and the twelve reanalysis products over China, i.e., (c)  
 55 ERA-Interim, (d) NCEP-R1, (e) MERRA, (f) JRA-55, (g) NCEP-R2, (h) MERRA2,  
 56 (i) ERA-20C, (j) ERA-20CM, (k) CERA-20C, (l) NOAA 20CRv2c, (m) NOAA

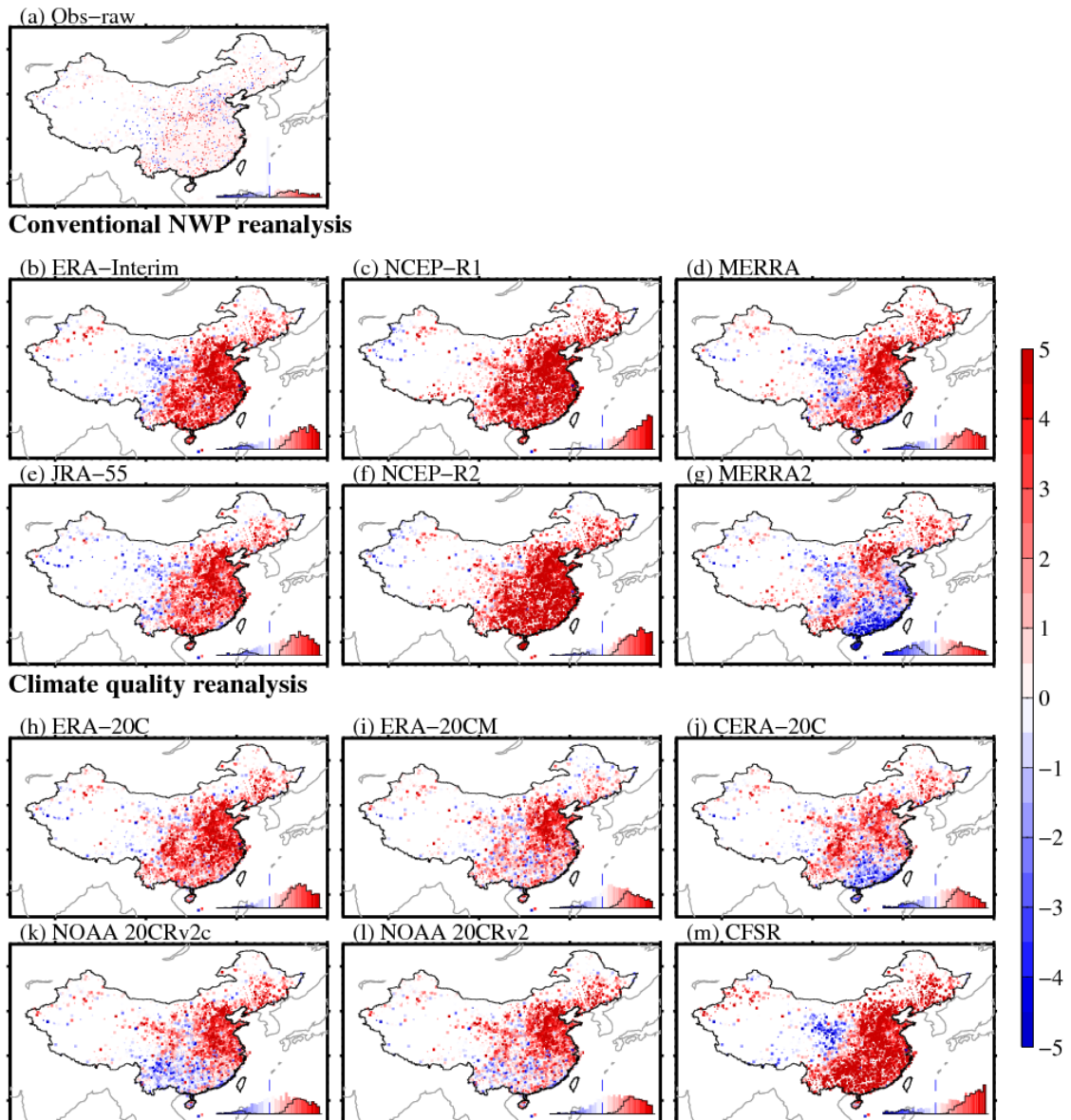
57 20CRv2 and (n) CFSR.



58

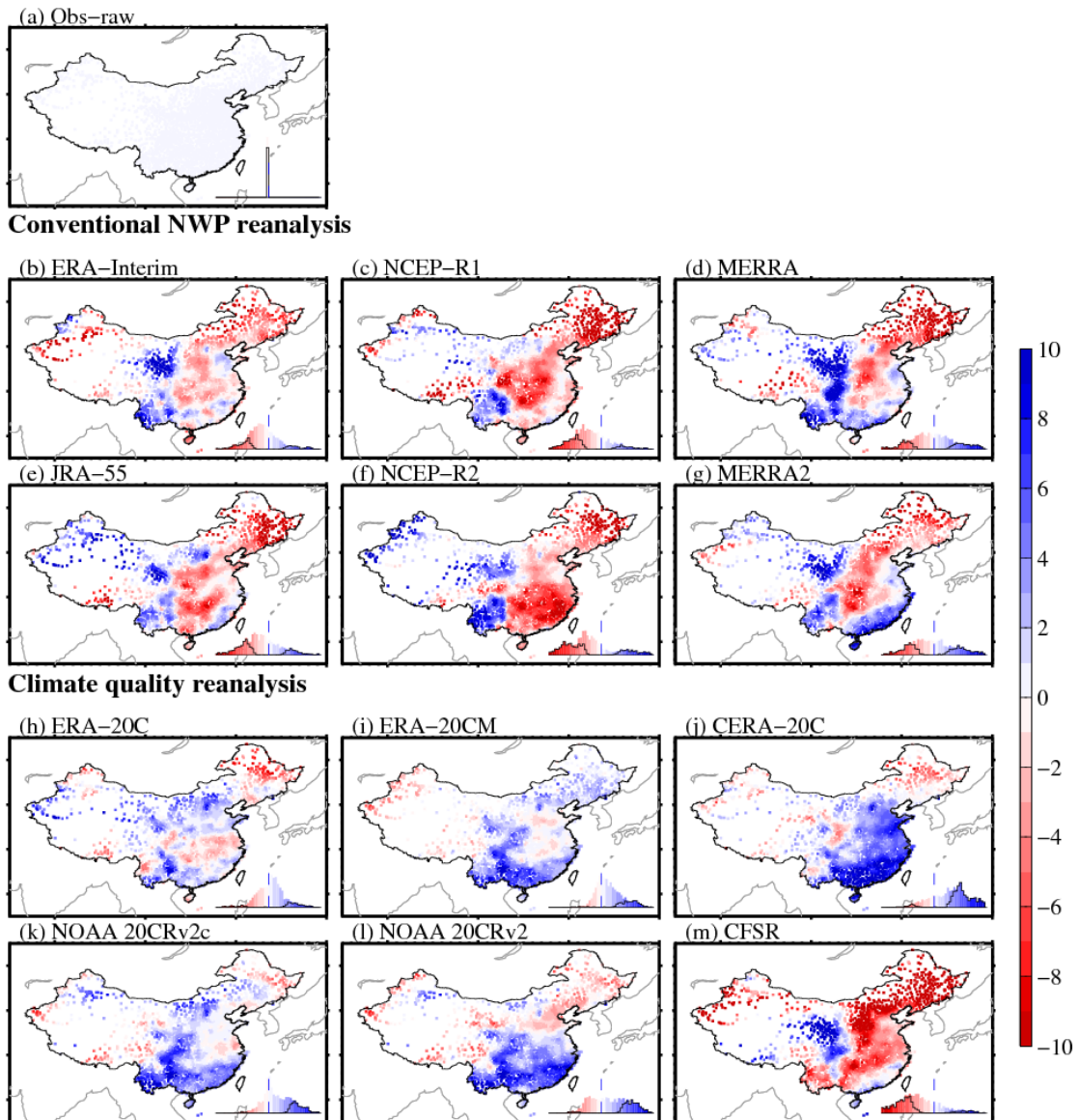
59 **Figure S7.** The same as Figure 5, but the colorbar is adjusted by adding mean value

60 (in red number within each subfigure).



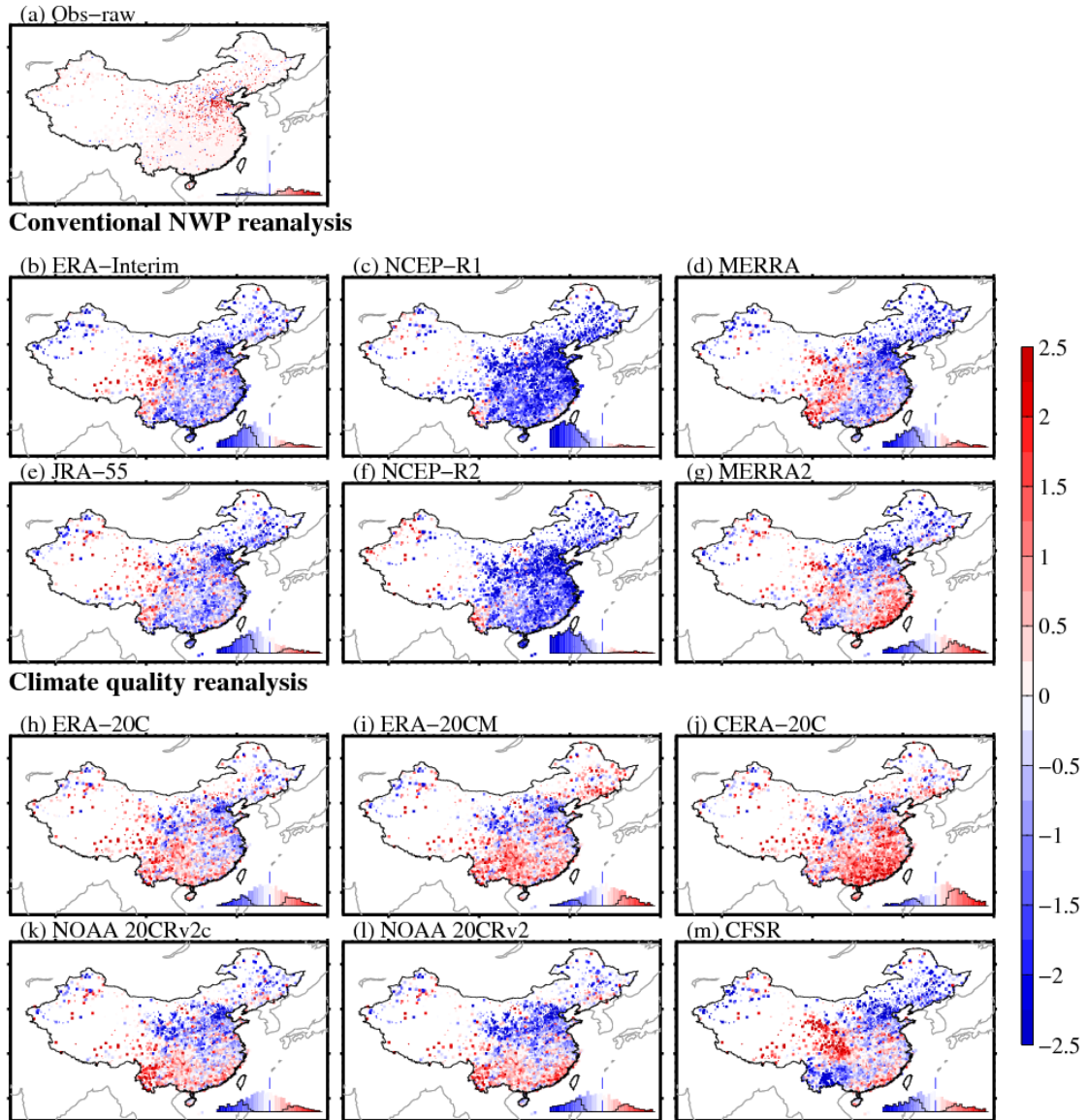
61

62 **Figure S8.** The simulated trend biases in surface incident solar radiation ( $R_s$ , unit:  
 63  $\text{W}\cdot\text{m}^{-2}/\text{decade}$ ) during the period 1979-2010 from the observations and the twelve  
 64 reanalysis products over China. The probability distribution functions of all the trends  
 65 are shown as colored histogram, and the black stairs are integrated from the trends  
 66 with a significance level of 0.05 (based on two-tailed Student's  $t$ -test).



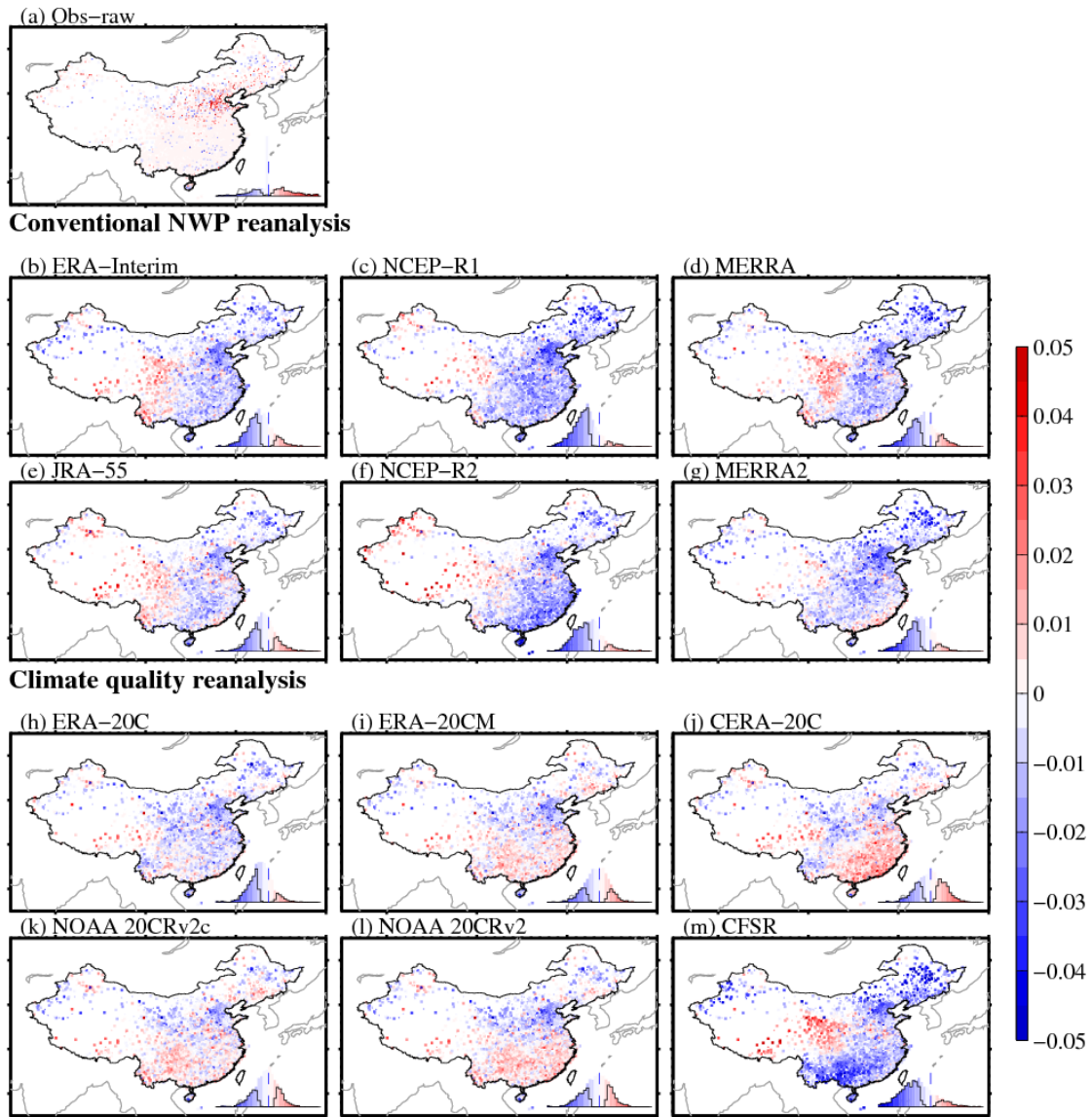
67

68 **Figure S9.** The simulated trend biases in the precipitation frequency (PF, unit:  
 69 days/decade) during the period 1979-2010 from the observations and the twelve  
 70 reanalysis products over China. The probability distribution functions of all the trends  
 71 are shown as colored histogram, and the black stairs are integrated from the trends  
 72 with a significance level of 0.05 (based on two-tailed Student's *t*-test).



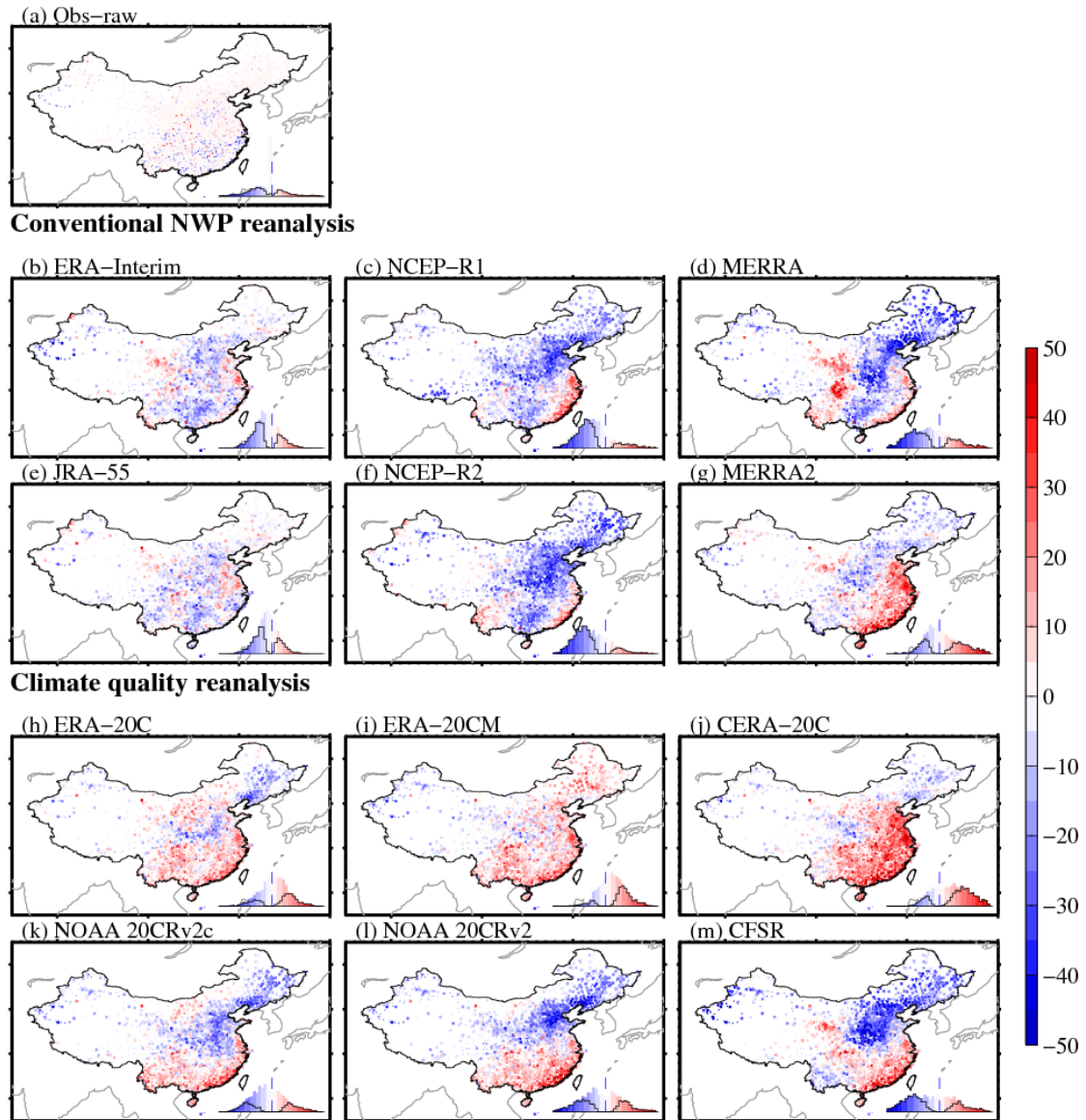
73

74 **Figure S10.** The simulated trend biases in surface downward longwave radiation ( $L_d$ ,  
 75 unit:  $\text{W}\cdot\text{m}^{-2}/\text{decade}$ ) during the period 1979-2010 from the observations and the  
 76 twelve reanalysis products over China. The probability distribution functions of all the  
 77 trends are shown as colored histogram, and the black stairs are integrated from the  
 78 trends with a significance level of 0.05 (based on two-tailed Student's  $t$ -test).



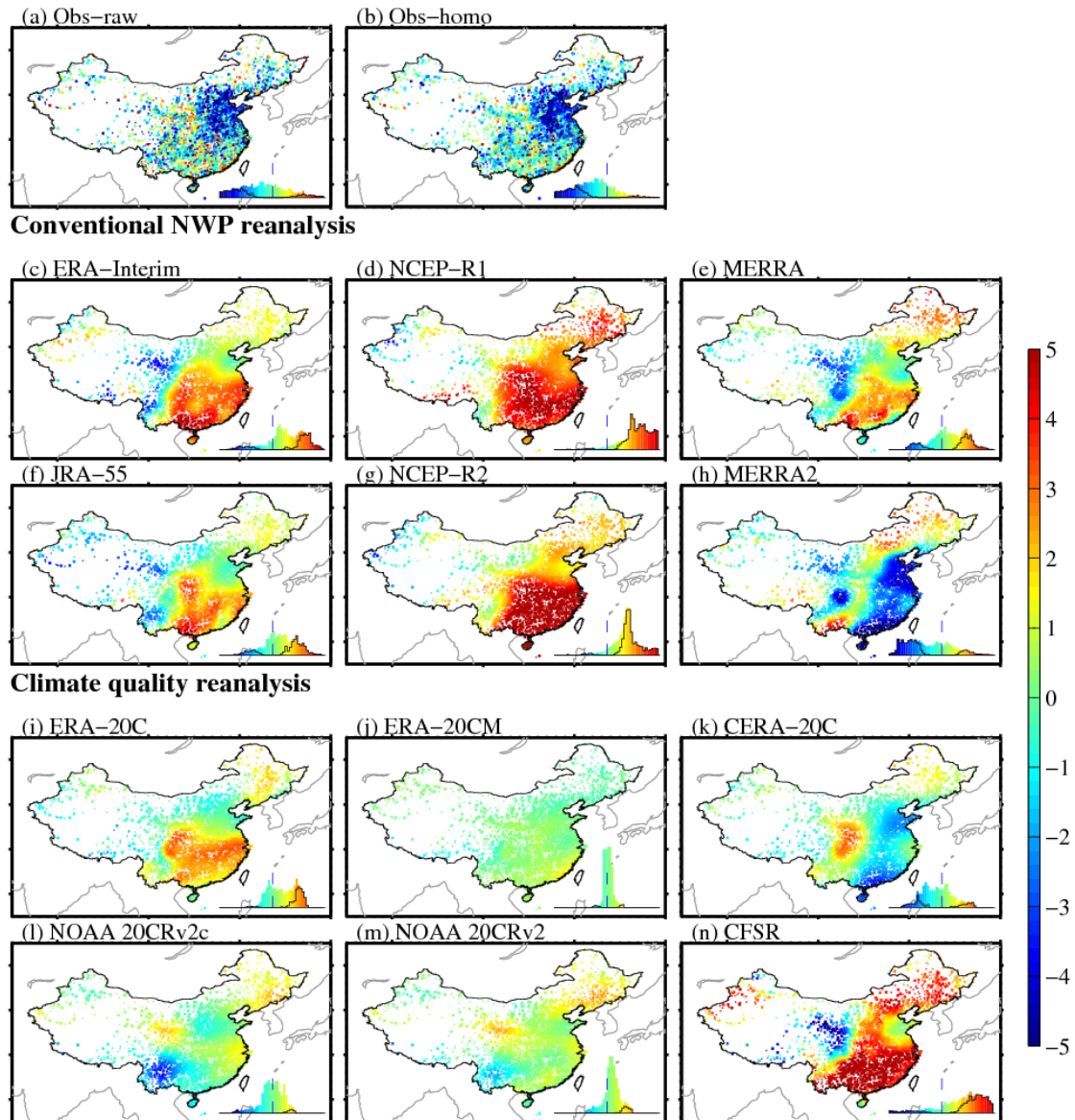
79

80 **Figure S11.** The simulated trend biases in cloud fraction (cld, unit: 1/decade) during  
 81 the period 1979-2010 from the observations and the twelve reanalysis products over  
 82 China. The probability distribution functions of all the trends are shown as colored  
 83 histogram, and the black stairs are integrated from the trends with a significance level  
 84 of 0.05 (based on two-tailed Student's  $t$ -test).



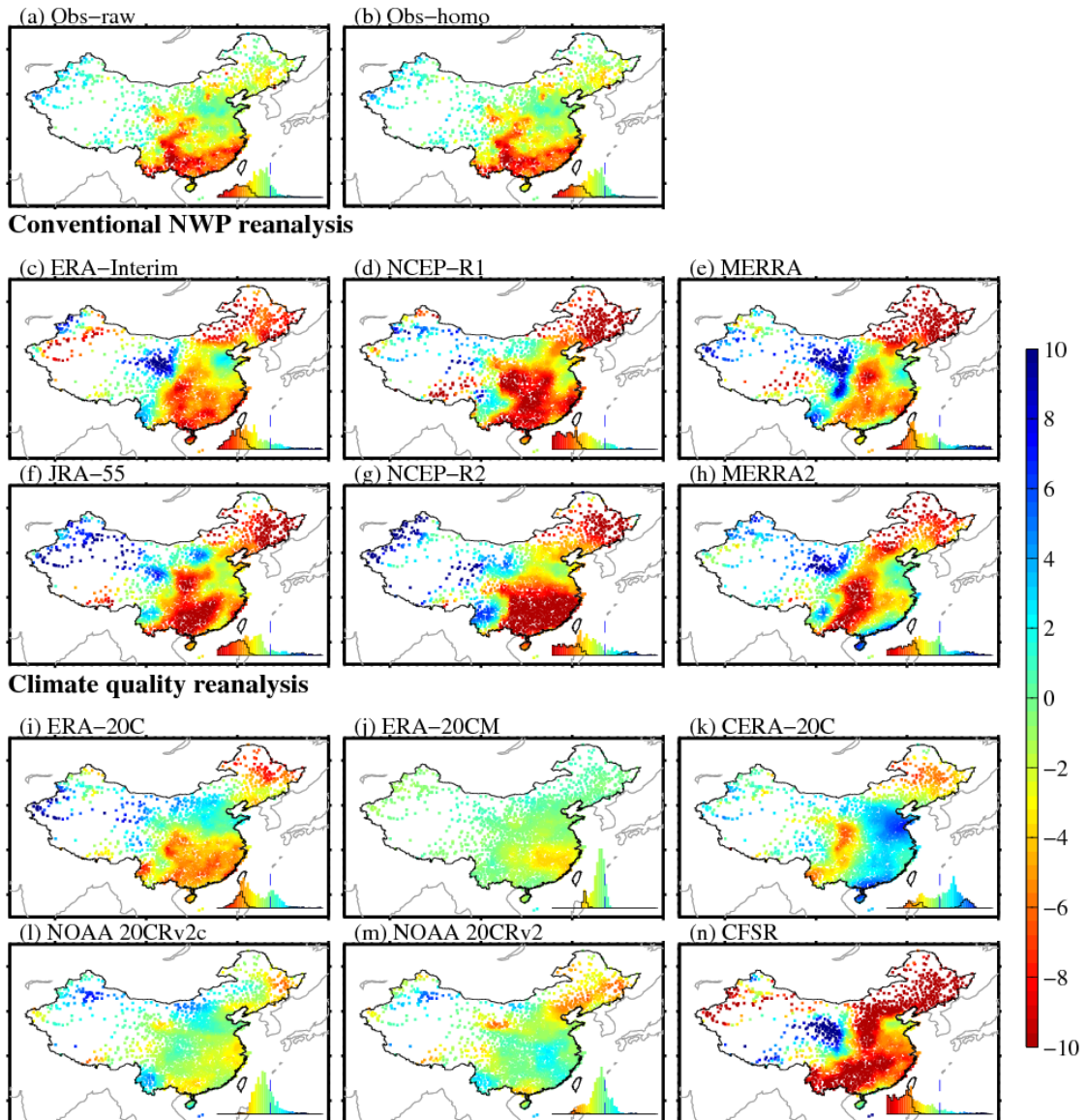
85

86 **Figure S12.** The simulated trend biases in the atmospheric water vapor (WVP, unit:  
 87 Pa/decade) during the period 1979-2010 from the observations and the twelve  
 88 reanalysis products over China. The probability distribution functions of all the trends  
 89 are shown as colored histogram, and the black stairs are integrated from the trends  
 90 with a significance level of 0.05 (based on two-tailed Student's *t*-test).



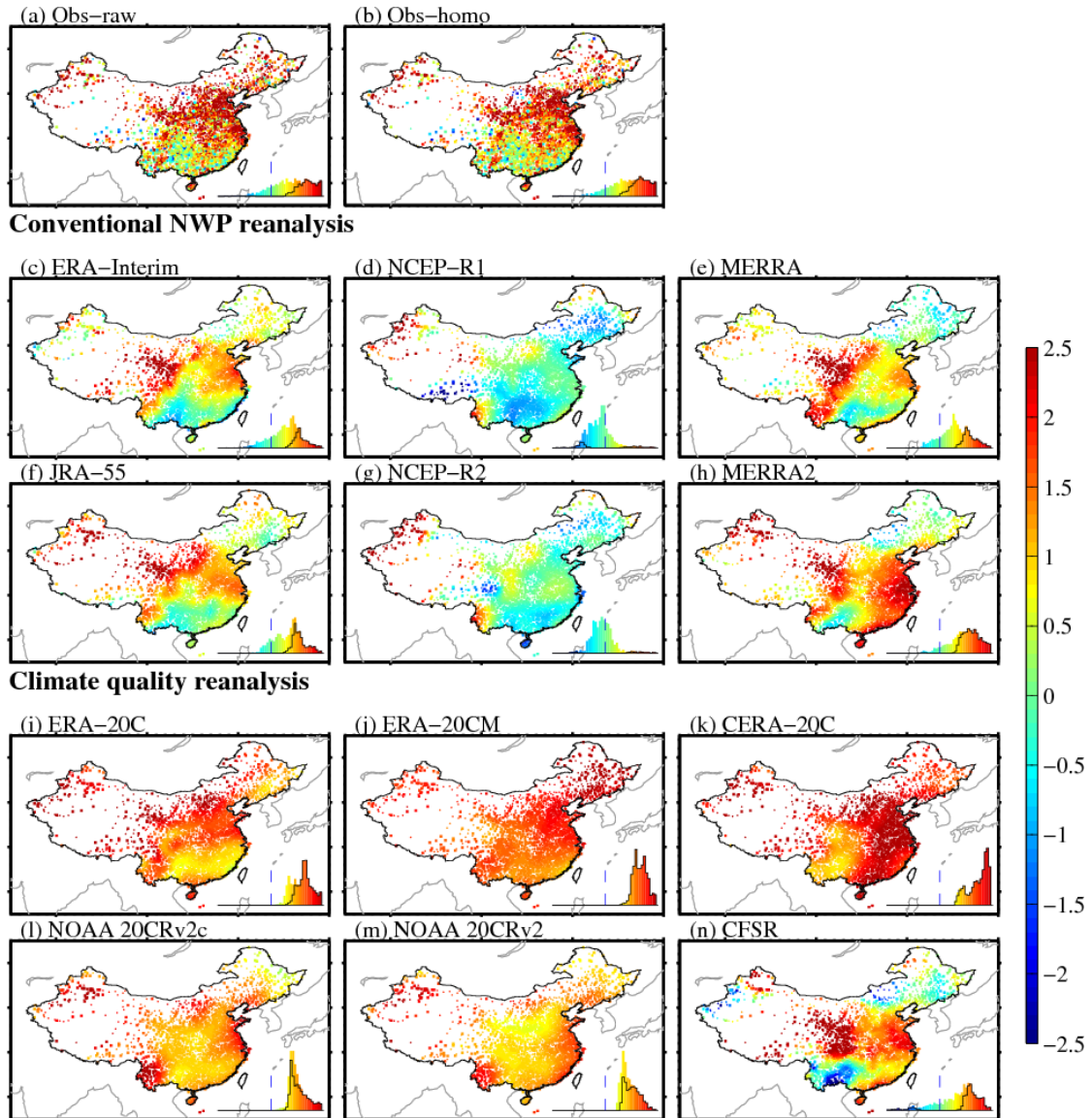
91

92 **Figure S13.** The trends in surface incident solar radiation ( $R_s$ , unit:  $W \cdot m^{-2}/decade$ )  
 93 during the period 1979-2010 from the observations and the twelve reanalysis products  
 94 over China. The probability distribution functions of all the trends are shown as  
 95 colored histogram, and the black stars are integrated from the trends with a  
 96 significance level of 0.05 (based on two-tailed Student's  $t$ -test).



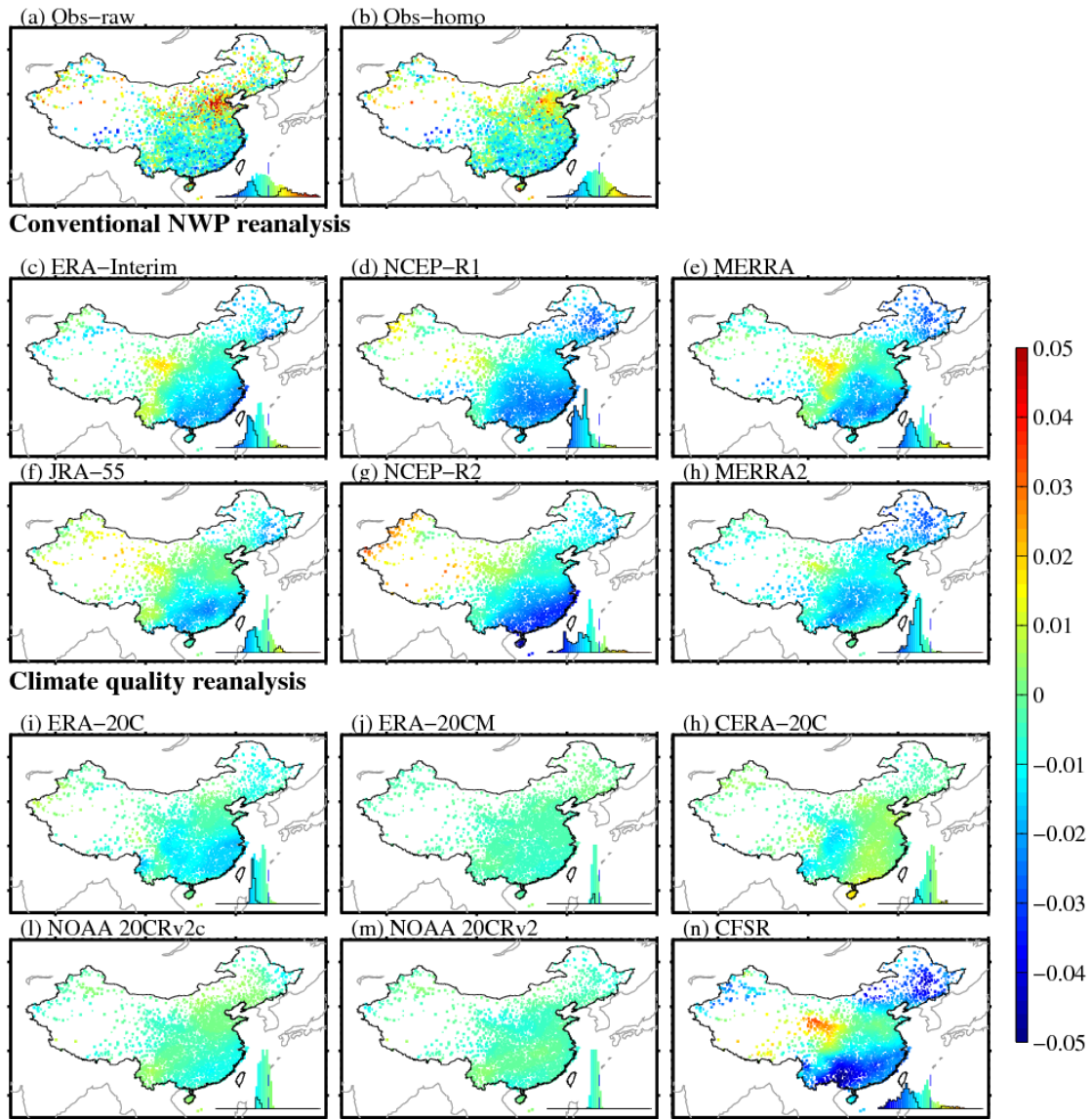
97

98 **Figure S14.** The trends in precipitation frequency (unit: days/decade) during the  
 99 period 1979-2010 from the observations and the twelve reanalysis products over  
 100 China. The probability distribution functions of all the trends are shown as colored  
 101 histogram, and the black stars are integrated from the trends with a significance level  
 102 of 0.05 (based on two-tailed Student's *t*-test).



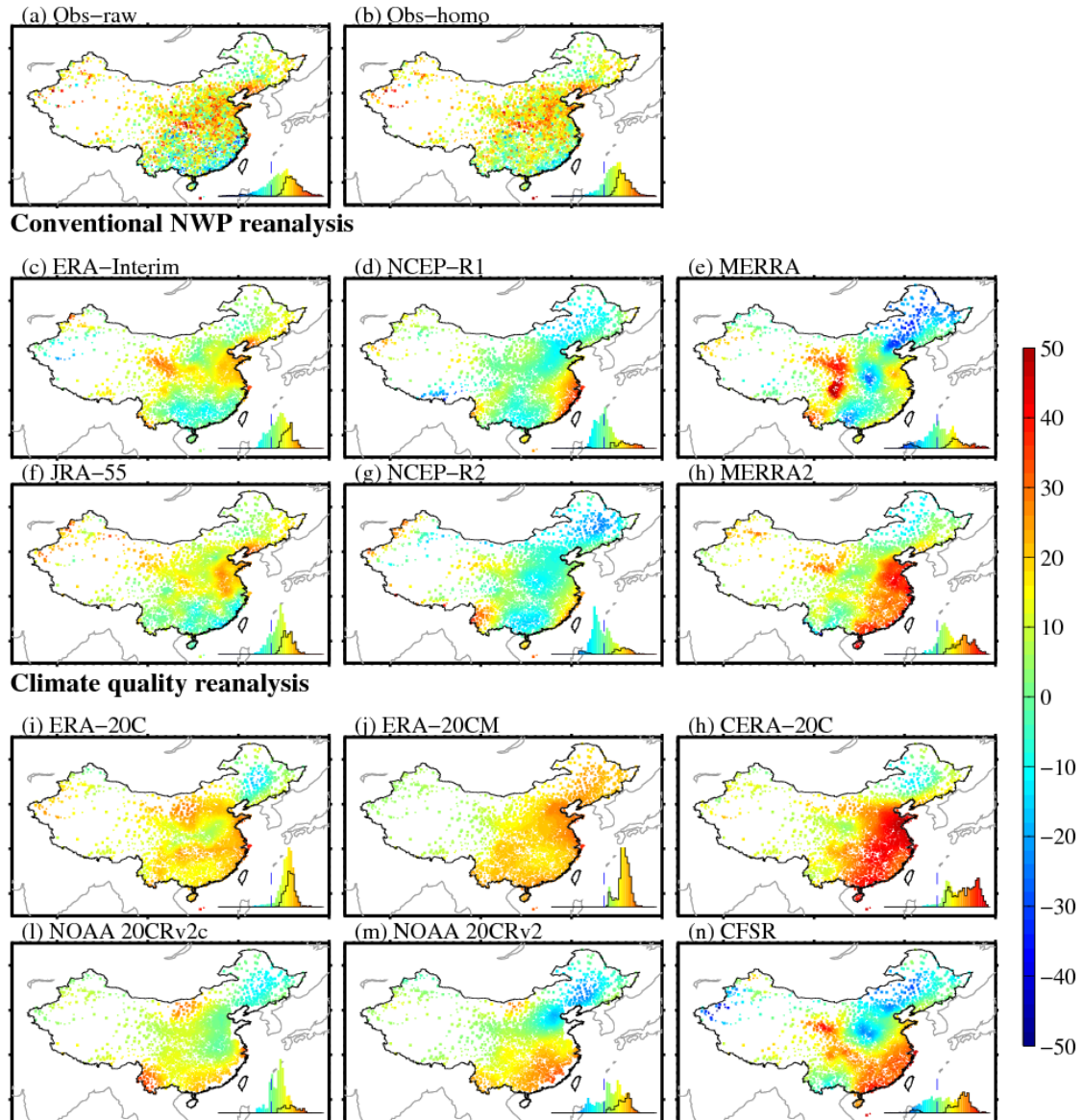
103

104 **Figure S15.** The trends in surface downward longwave radiation ( $L_d$ , unit:  
 105  $\text{W}\cdot\text{m}^{-2}/\text{decade}$ ) during the period 1979-2010 from the observations and the twelve  
 106 reanalysis products over China. The probability distribution functions of all the trends  
 107 are shown as colored histogram, and the black stairs are integrated from the trends  
 108 with a significance level of 0.05 (based on two-tailed Student's  $t$ -test).



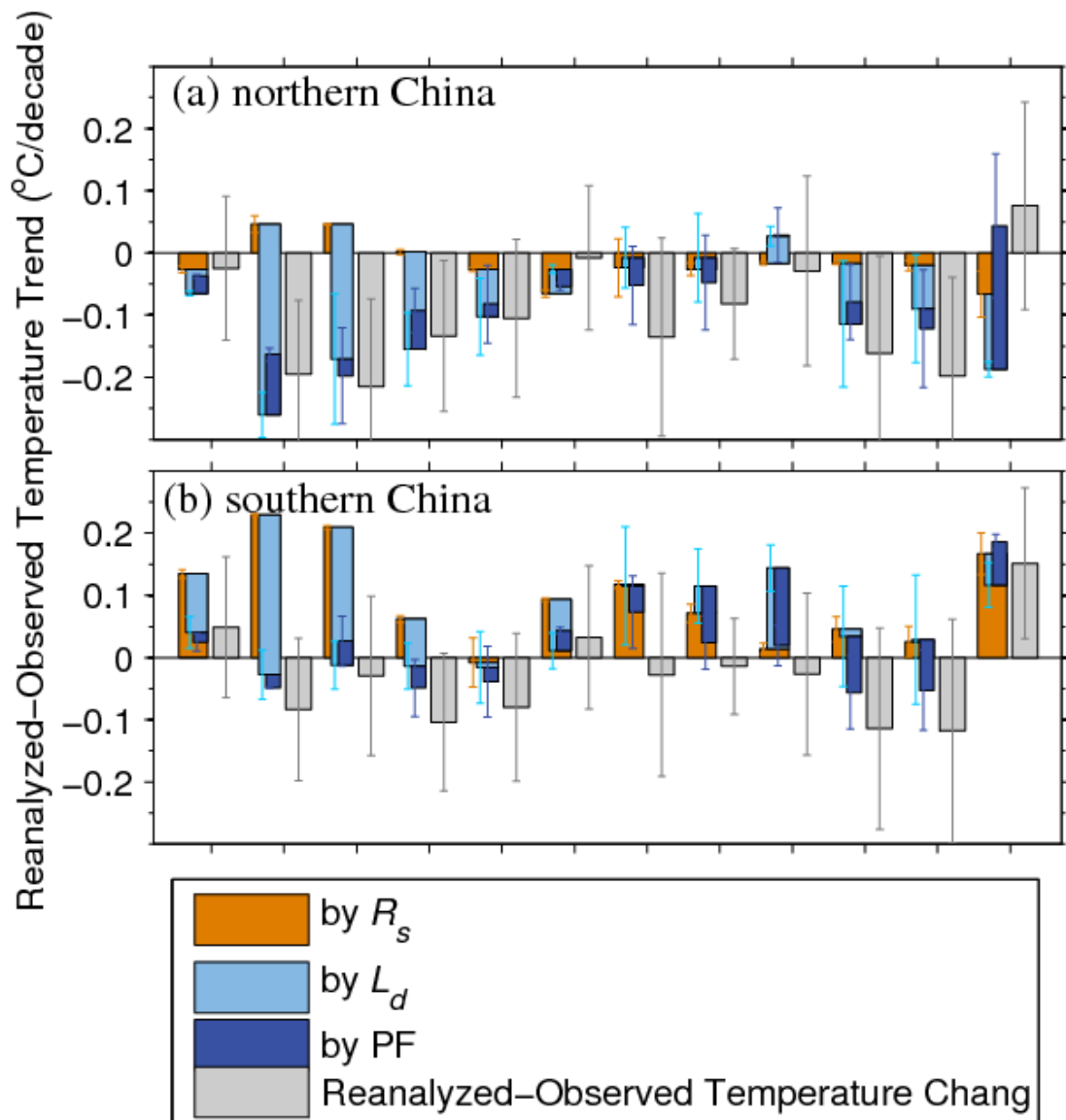
109

110 **Figure S16.** The trends in cloud fraction (cld, unit: 1/decade) during the period  
 111 1979-2010 from the observations and the twelve reanalysis products over China. The  
 112 probability distribution functions of all the trends are shown as colored histogram, and  
 113 the black stairs are integrated from the trends with a significance level of 0.05 (based  
 114 on two-tailed Student's *t*-test).



115

116 **Figure S17.** The trends in the atmospheric water vapor (WVP, unit: Pa/decade) during  
 117 the period 1979-2010 from the observations and the twelve reanalysis products over  
 118 China. The probability distribution functions of all the trends are shown as colored  
 119 histogram, and the black stars are integrated from the trends with a significance level  
 120 of 0.05 (based on two-tailed Student's *t*-test).

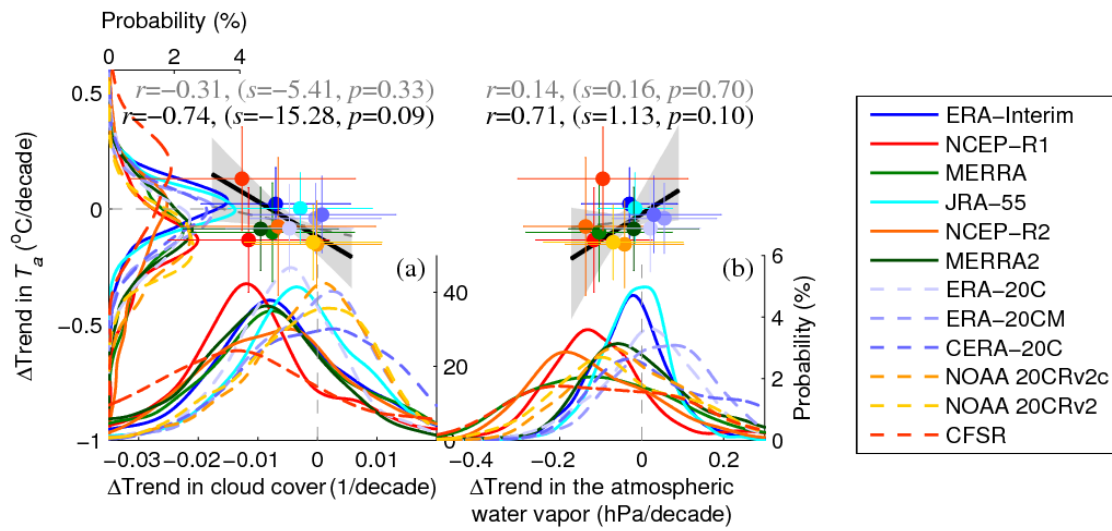


121

122 **Figure S18.** The same as Figure 7, but over northern China (including the Tibetan

123 Plateau, Northwest China, Loess Plateau, Northeast China) and southern China

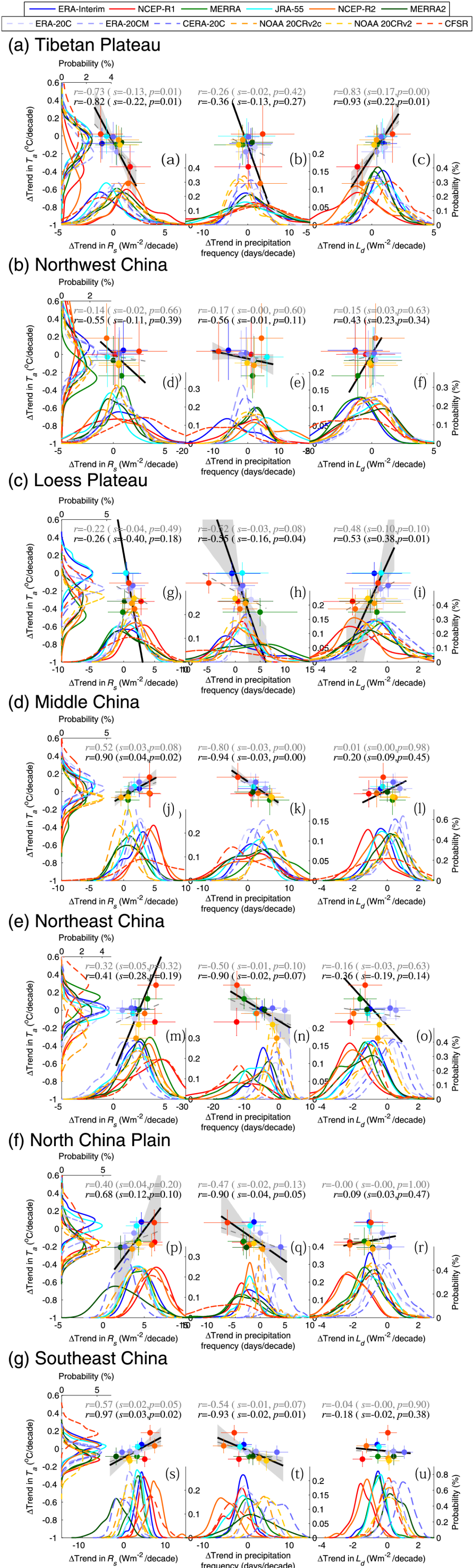
124 (including the North China Plain, Middle China and Southeast China).



125

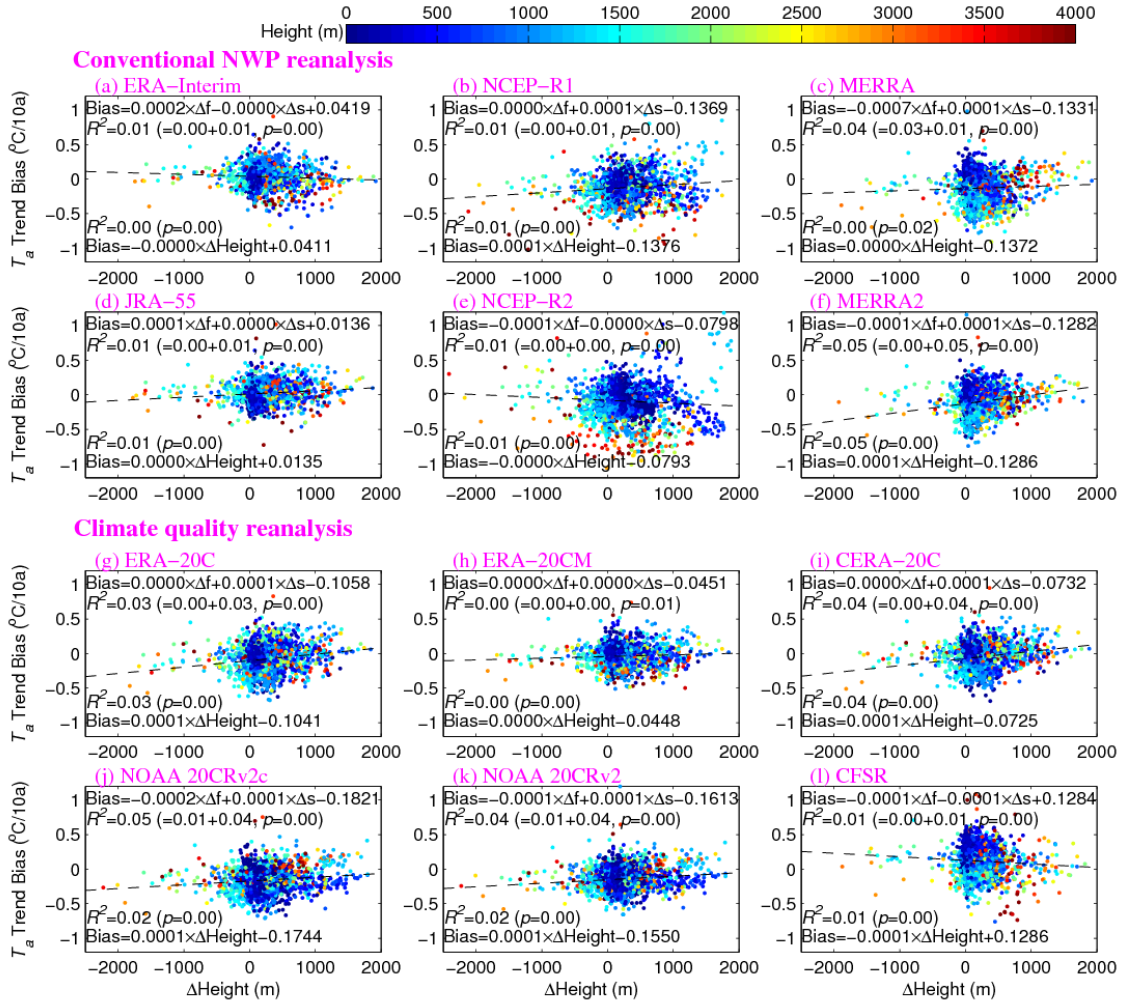
126 **Figure S19.** The same as Figure 8, but for the simulated biases in (a) cloud fraction

127 and (b) the atmospheric water vapor.



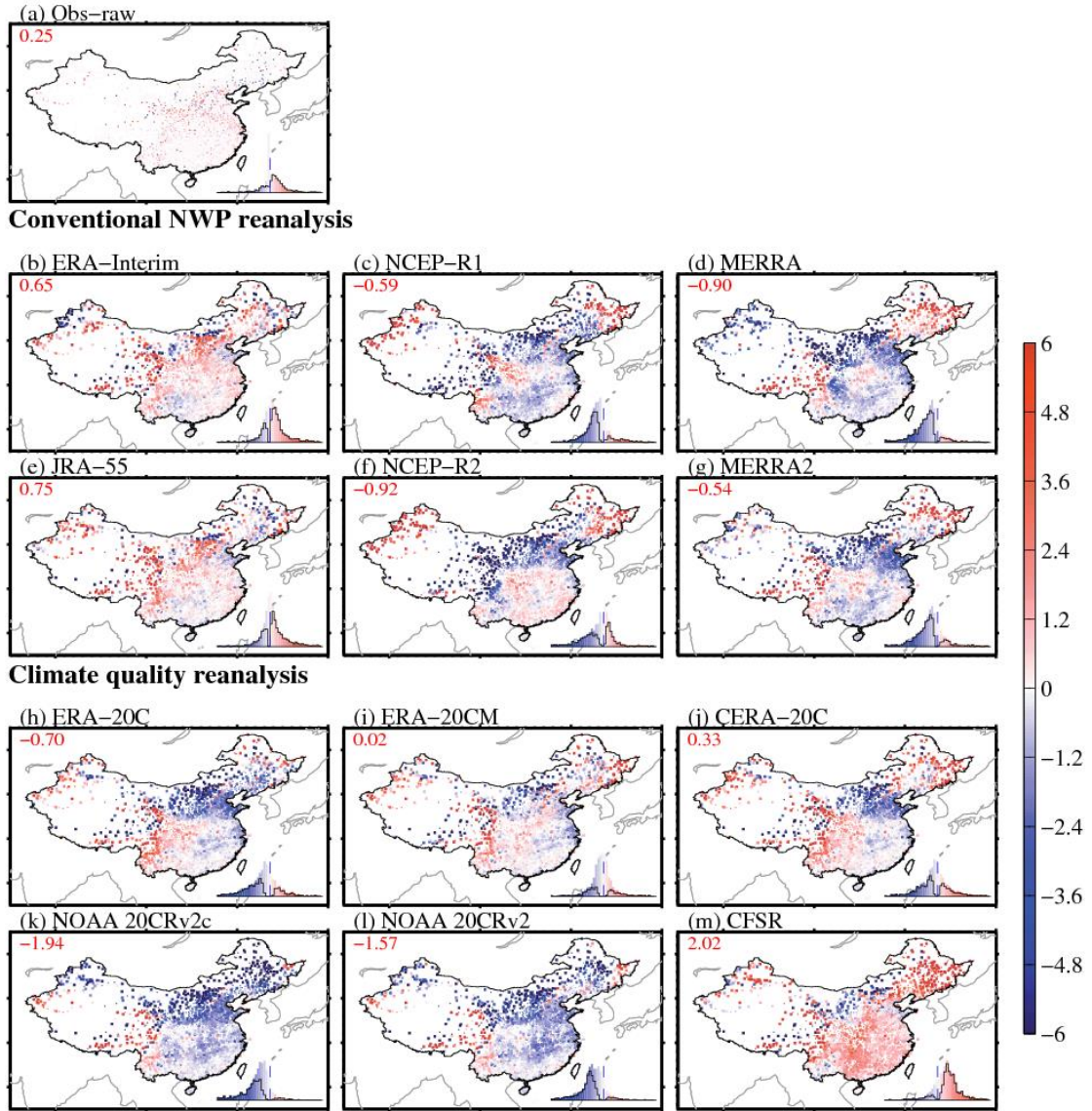
128

129 **Figure S20.** The same as Figure 8, but over China's subregions.



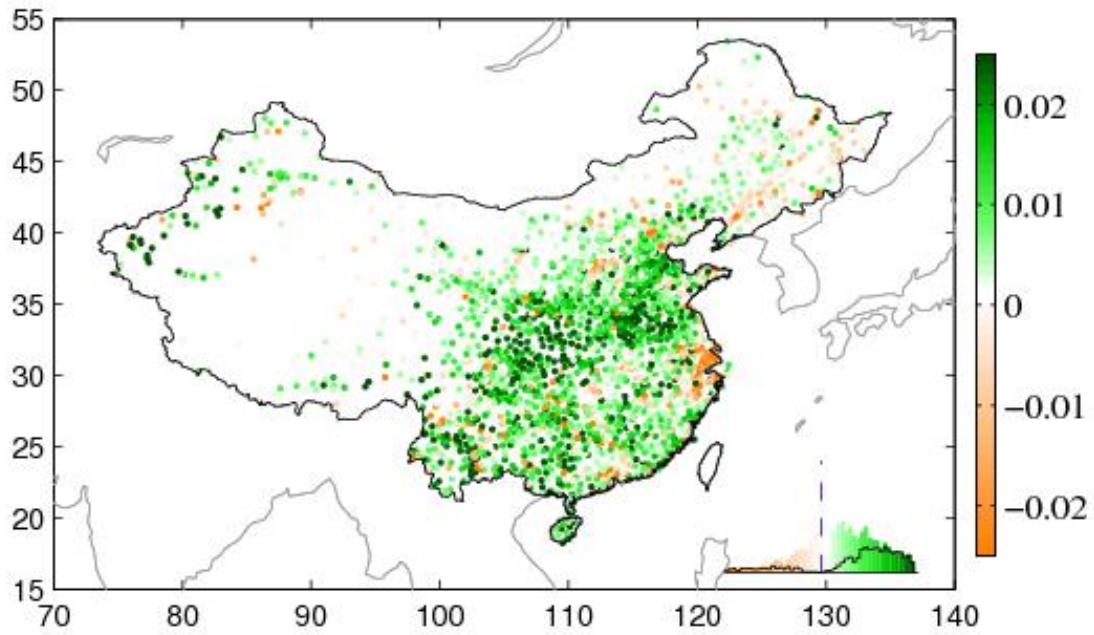
130

131 **Figure S21.** The same as Figure 2, but for the trend biases in surface air temperature  
 132 ( $T_a$ , unit:  $^{\circ}\text{C}/\text{decade}$ ). The elevation difference between model and stations actually  
 133 influence the trend bias in  $T_a$ , but can not explain the spatial pattern in the trend bias  
 134 in  $T_a$  ( $R^2=0.02$ ), mainly due to the nearest warming within the lowest atmospheric  
 135 boundary layer. Moreover, compared the same-grid models (NOAA 20CRv2c vs.  
 136 NOAA 20CRv2, MERRA vs. MERRA2, NCEP-R1 vs. NCEP-R2 and ERA-20C vs.  
 137 ERA-20CM), we found the one statistically correlates with the elevation difference  
 138 but the other does not, which implies that this statistical correlation should not be  
 139 physical significance. Additionally, the elevation difference does not change with  
 140 time.



141

142 **Figure S22.** The same as Figure 5, but for the normalized trends in surface air  
 143 temperature (%/decade). The normalized trends can exclude the impact of absolute  
 144 value of temperature on the trends. One can find that the spatial patterns in the  
 145 normalized trends is very near to those of the trends, implying the impact of  
 146 difference in absolute value of temperature due to the site-to-grid inconsistency can be  
 147 neglected. This result is consistent with that based on Figure S20.



148

149 **Figure S23.** The trend in vegetation growth depicted by Normalized Difference  
 150 Vegetation Index (NDVI, unit: 1/decade) during the period 1981-2010 from the  
 151 observations and the twelve reanalysis products over China. The probability  
 152 distribution functions of all the trends are shown as colored histogram, and the black  
 153 stairs are integrated from the trends with a significance level of 0.05 (based on  
 154 two-tailed Student's *t*-test).